MODELING PLASMONIC SOLAR CELLS WITH NOBLE METAL NANOPARTICLES USING THE FINITE DIFFERENCE TIME DOMAIN METHOD

M. M. SHABAT[1,*], S. A. NASSAR[1], H. G. ROSKOS[2]

[1] Department of Physics, School of Science, Islamic University of Gaza, P.O. Box 108, Gaza Strip, Palestine
[2] Physikalisches Institut, Johann Wolfgang Goethe-Universität, Max-von-Laue-Straße 1, D-60438 Frankfurt am Main, Germany
[*] Corresponding author, *email*: shabatm@googlemail.com

Received June 3, 2020

Abstract. Light trapping in solar cells can be enhanced exploiting the concept of surface plasmons in nanostructures. A new type of light trapping structure utilizing nanoparticles of noble metals is investigated for the absorption enhancement in solar cell modules. The *finite-difference time-domain* (FDTD) method is used to simulate and compute the absorption spectra of the proposed solar cell structure.

Key words: Thin-film solar cell, plasmonics, metal nanoparticles, FDTD method, absorption, reflection

1. INTRODUCTION

Solar cells for photovoltaics, converting sunlight directly into electrical power, are sources of green, safe, renewable, user-friendly, and clean energy [1–7]. Most solar cells depend on silicon as the light-absorbing material [2–18] due to its stability, well-developed technology, non-toxicity, and abundance in nature. However, silicon suffers from an indirect energy bandgap. The resulting low absorption cross-section of light in the visible and infrared spectral range can severely limit the performance of the solar cell. For that reason, many researchers are shifting to other materials with direct-gap optical transitions in order to increase the efficiency of the proposed solar cells. Alternatively, one can enhance the light absorption in the Si devices if this is associated with an enhanced generation rate of electron-hole pairs, which contribute to the photocurrent in the device. Metal *nanoparticles* (NPs), *e.g.* fabricated from silver (Ag), gold (Au) or aluminum (Al), are very well suited for this purpose. They combine strong light absorption originating from the excitation of localized surface plasmons [8, 9, 11–16] with the generation of a localized electric field of the plasmon modes that strongly overlaps with the surrounding Si material for efficient generation of electron-hole pairs by interband absorption in Si. The excitation of the local plasmon field of the NPs

effectively acts like an increase of the path length of light in Si, leading not only to an increase of the efficiency of the solar cells, but also to lower manufacturing costs because of a reduced amount of Si needed.

NPs in solar cells are not only of interest as absorbers but also find use for the control and optimization of the cells' dielectric properties mainly in order to reduce reflection losses. The effect of SiNPs in antireflection coatings of waveguide structures has been investigated and optimized [12, 17]. Other multilayered waveguide structures containing NP [8–16] have numerically been investigated showing the importance of NP in minimizing light reflection of such structures. The absorption properties of the cells were not in the foreground of these studies. In contrast, the present work focuses on the effects of the NPs on the absorption spectra in the proposed solar cell structure.

Solar cells are complex structures [2–21]. Their design needs highly sophisticated numerical techniques, and several methods are effectively in use to analyze and minimize reflection and maximize both absorption and transmission. Notably, the transfer matrix method (TMM) [20–22] and the *finite-difference time-domain* (FDTD) calculations [23–28] are familiar techniques which have been implemented to investigate these complex structures. Here, we employ the FDTD method.

The paper is organized as follows: in Sec. 2, the device design and the underlying electromagnetic theory are presented. Section 3 is dedicated to the numerical simulations and their results, and Sec. 4 draws the conclusions of this work.

2. DESIGN AND THEORY

The proposed unit cell of the plasmonic thin solar cell containing NPs for the generation of localized surface plasmons by light absorption is illustrated in Fig. 1. The four-layered structure consists of a top layer formed by the metal NPs (Ag, Al, Au; for a discussion of this layer, see below), an *indium tin oxide* (ITO) layer carrying the NPs, the active layer (absorbing material: amorphous silicon, a-Si), and the substrate (SiO_2) with thicknesses of d_0, d_1, d_2, and d_3, respectively. The lateral spatial period is P. The incident plane-wave light is p-polarized (TM mode) and injected into the structure *via* the metal NPs. *Perfectly matched layer* (PML) boundary conditions are employed at the top and the bottom of the solar cell structure, while *periodic boundary conditions* (PBCs) are imposed at the left and right sides of the unit cell. The geometrical parameters of the device are set as $d_0 = 25$ nm, $d_1 = 25$ nm, $d_2 = 120$ nm, $d_3 = 40$ nm, and $P = 200$ nm. The properties of the materials of the solar cell structure are taken from Refs. [29, 30].

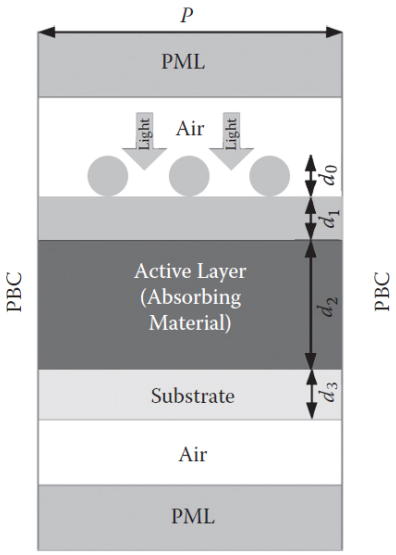

Fig. 1 – Schematic diagram of the plasmonic solar cell with metal nanoparticles.

We assume here vertical incidence of the light (propagation direction: *y*-direction) whose spectral wavelength range is 300–1200 nm. We furthermore assume that light scattering by the NPs is negligible and that the NP arrangement can be treated as a thin, homogeneous film, as mentioned above. The NPs are supposed to be spherical in shape, identical in size and to form a monolayer of particles, with d_0, the thickness of the monolayer, representing also the diameter of each NP. Following Refs. [17, 31–33], the permittivity of the film can be described in an effective-medium picture by

$$\varepsilon_{eff} = \varepsilon_b \frac{\varepsilon_i(1+2f)+2\varepsilon_b(1-f)}{\varepsilon_i(1-f)+\varepsilon_b(2+f)} \tag{1.1}$$

where ε_b is the permittivity of the host material (here: air), ε_i is the permittivity of the NPs' materials, and f is the volume fraction of the particles in the host medium. This continuum model describes the absorption of light by dielectrically interacting spheres with a diameter much smaller than the wavelength of the light [31].

For the permittivity of the metals forming the NPs, we use the following values [29, 30, 32, 33]:

For Ag: $\varepsilon_{Ag} = -16.074 + j\,0.44233$, for Al: $\varepsilon_{Al} = -50.038 + j\,18.141$, and for Au: $\varepsilon_{Au} = -9.3875 + j\,1.5292$.

All values given above are for a wavelength of 600 nm, the center of the visible spectral range and close to the peak of the sunlight spectrum as measured on

the ground, where it is especially desirable to improve the performance of thin-film Si solar cells. The wavelength dependence of the permittivity is not taken into account.

The volume fraction *f* of the NPs can be expressed as [17, 31–33]:

$$f = \frac{N_p \times V_p}{V_{layer}}, \tag{1.2}$$

where $V_{layer} = L \times l \times d$, with L being the length of the silicon solar cell's surface, l its width, and $d = d_0$. For simplicity, we take $L = l = d_0 = 25\,\text{nm}$. The volume of each NP is $V_p = 4\pi r^3/3$, where r is the radius of the NP ($d_0/2$). For the chosen length and width of the considered surface, the effective number of particles N_p on that surface is always smaller than 1. The volume fraction is used as the density parameter in the following. If $f = 0$, the NP layer is non-existent and the incident light impinges from the air directly onto the ITO film.

For these non-magnetic materials without free charges and currents, the FDTD method is used to solve:

$$\nabla \times E = -\mu_0 \frac{\partial H}{\partial t} \quad \text{(Faraday's law)} \tag{1.3}$$

$$\nabla \times H = \varepsilon_0 \varepsilon \frac{\partial E}{\partial t} \quad \text{(Ampere's law)} \tag{1.4}$$

where E is the electric field, H is the magnetic field, ε is the permittivity of the respective material, and ε_0 and μ_0 denote the electric and magnetic field constants. For the numerical calculations, we employ the FDTD software [34]. We evaluate the absorbance spectra, *i.e.* the power absorption coefficient $A(\lambda)$, determined from the calculated reflectance and transmittance spectra by the application of the law of conservation of energy as in Refs. [10, 12, 35]: $A(\lambda) = 1 - R(\lambda) - T(\lambda)$, where λ is the wavelength of the light.

3. SIMULATION RESULTS

Three types of NP materials, silver (Ag), gold (Au), and aluminum (Al) are considered in the following. For each material, Figs. 2–4 show the respective absorption spectra of the proposed solar cell structure for different values of the volume fraction *f* of the NPs.

Figure 2 displays spectra for Ag. Without NPs in the structure, the spectral features are dominated by the absorption properties of Si, *i.e.*, the rise of the

absorption of Si with decreasing wavelength of the light (indirect bandgap at 1130 nm, direct gap at 370 nm). The trend is not smooth, however, but rather modulated by light interference in the layered structure. With the NPs in the structure, the peaks and valleys of the modulation shift, this being a consequence of the change of the refractive index by the NPs. In addition, one observes an overall increase of absorption with rising volume fraction of the NPs.

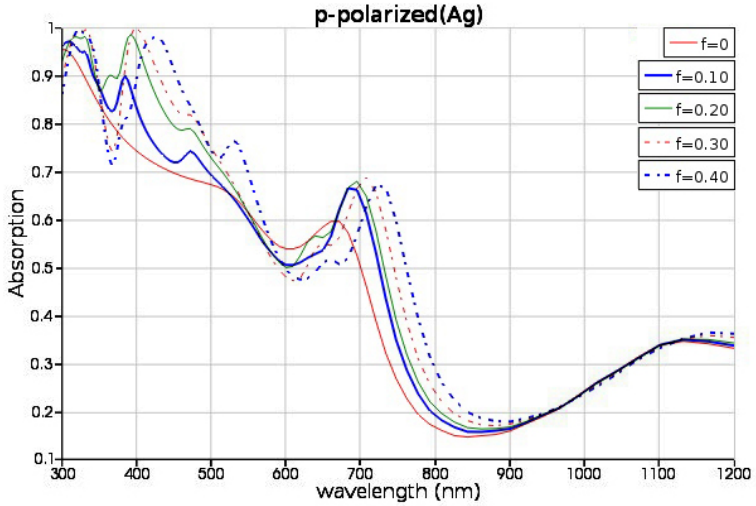

Fig. 2 – Absorption spectra of the proposed solar cell structure with Ag nanoparticles in the top layer with different values of (f =0, 0.10, 0.20, 0.30, 0.40) and Si substrate.

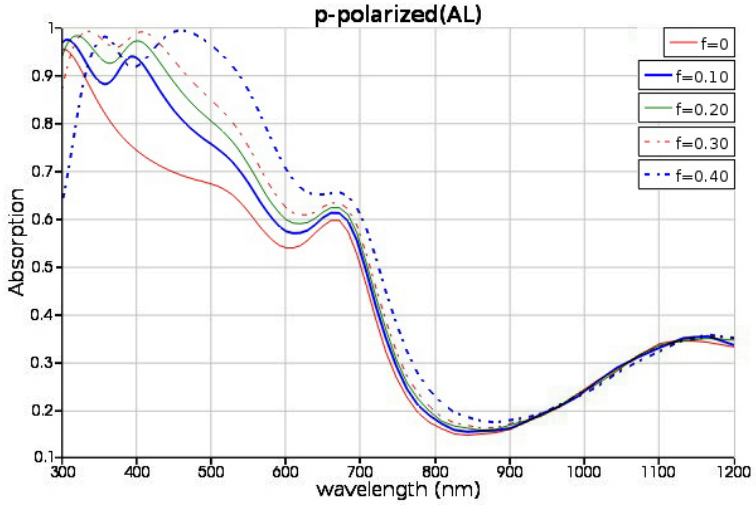

Fig. 3 – Absorption spectra of the proposed solar cell structure for different values of the volume fraction of Al nanoparticles.

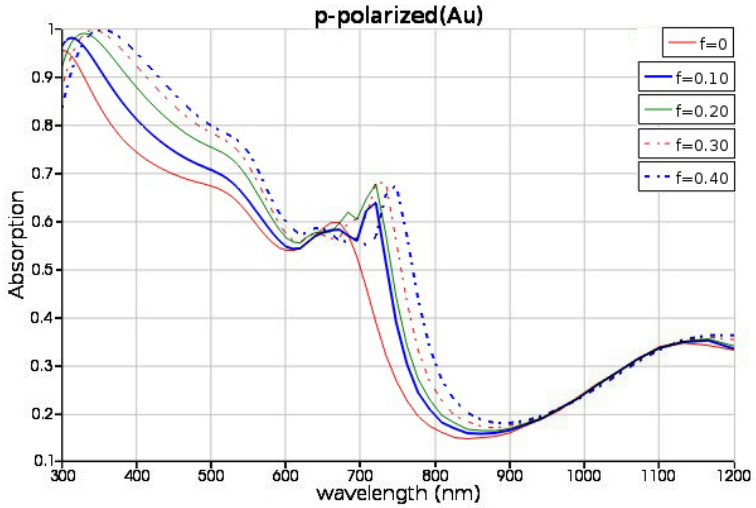

Fig. 4 – Absorption spectra of the proposed solar cell structure for different values of the volume fraction of Au nanoparticles.

Figures 3 and 4 display the corresponding absorption spectra for Al NPs (Fig. 3) and Au NPs (Fig. 4). Of all three noble metals and for a given volume fraction of the NPs, Al produces the strongest effect on the absorption especially around 600 nm, the wavelength region of special interest. This is a consequence of the fact that the absolute value of both the real and imaginary parts of the permittivity are highest for Al, which translates into the largest extinction coefficient k and refractive index n of the three noble metals: k = 4.01, 7.19, 3.07 for Ag, Al, Au, respectively, and n = 0.06, 1.26, 0.25 accordingly.

In the following, numerical simulations are performed for solar cells with five different configurations, and the neat figures display the magnetic field intensity profiles for all the configurations at short and long wavelength peaks taken from Figs. 2–4.

Figure 5 and 6 shows the H_z field distributions at the absorption peaks in Figs. 2, 4. For comparison, the magnetic intensity distribution for the reference cell is given in Figs. 5, 6 (a and f). It is clear that the magnetic intensity enhancements as well as the strong energy flows into and distributes in the lower side of the NP's (at $y < 0$), which further confirms the forward scattering caused by the Localized surface plasmon resonance, LSPR. In addition, the light scattered by the Ag NPs and propagated at different angles will increase the light path in the active layer, which also contributes to the absorption enhancement. At short wavelength in Figs. 5, 6 (b-e) the magnetic field is more concentrated in the ITO layer (from $y = 0$ to $y = –25$ nm) and extends below the ITO layer. For long wavelengths, Ag NP's contribute to the absorption enhancement. The concentrated field at the absorption

layer due to the Bloch mode-like diffraction patterns with a periodicity in the horizontal *x*-direction can be observed clearly in Figs. 5, 6 (g-j).

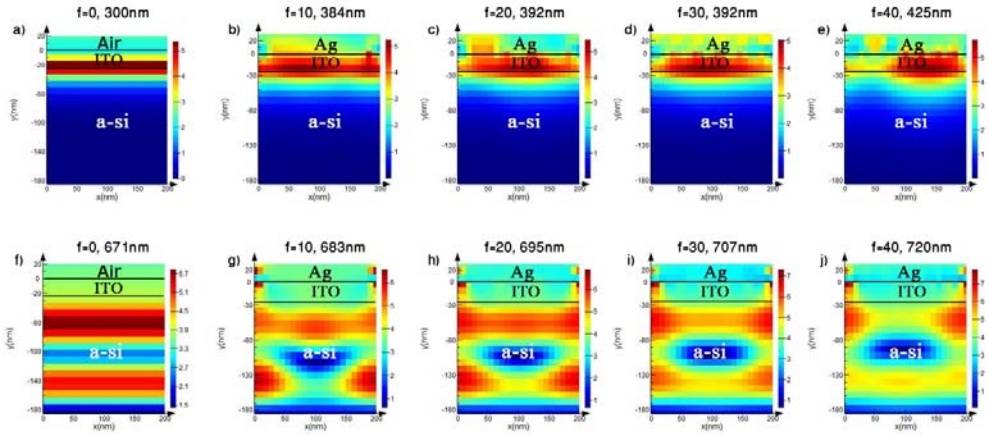

Fig. 5 – Magnetic field H_z distribution at short and long wavelengths for Ag nanoparticles on top of ITO in the form of nano-spherical with varying volume fraction in solar structure for TM mode of incident light.

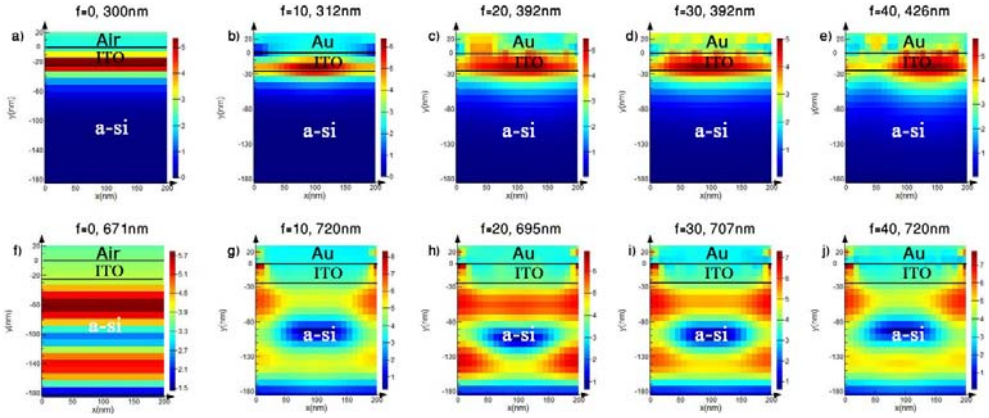

Fig. 6 – Magnetic field H_z distribution at short and long wavelengths for Au nanoparticles on top of ITO in the form of nano-spherical with varying volume fraction in solar structure for TM mode of incident light.

The reference structure is compared to structures including Al NP's. One should note that at long wavelength range, the absorption peaks in Fig. 3 illustrate the shorter lifetime of the photons trapped in the solar cell structure. This is referring to increased line width of the corresponding absorption peaks in Fig. 3 compared with Au and Ag NP's in Figs. 2, 4. At short wavelength in Fig. 7 (b–e), the magnetic field is more concentrated in the ITO layer (from $y = 0$ to $y = 25$ nm) and extends below the ITO layer specially in Fig. 7e.

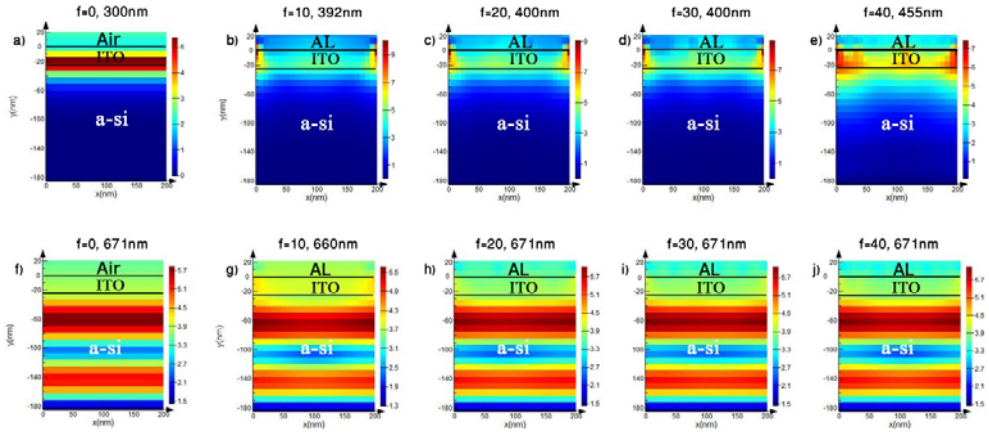

Fig. 7 – Magnetic field H_z distribution at short and long wavelengths for Al nanoparticles on top of ITO in the form of nano-spherical with varying volume fraction in solar structure for TM mode of incident light.

Significant new results have been displayed in Tables 1 and 2 showing the compression of the absorption, reflection, and transmission, respectively. Table 1 shows clearly the compression of the absorption spectra due to different types of nanoparticles volume fraction (Ag, Au, Al) in the front layer of the solar cell structure. Table 1 also shows that the increase of the nanoparticles volume fraction of aluminum (Al) leads to a larger absorption than that corresponding to the noble metals Ag and Au.

Table 1

The absorption of metal nanoparticles (Ag, Al, Au) with different values of the volume fraction (f)

Absorption %	Ag	Al	Au
$f = 0$	62.1855%	62.1855%	62.1855%
$f = 0.10$	65.2078%	68.4649%	66.5391%
$f = 0.20$	68.5668%	71.251%	69.7818%
$f = 0.30$	68.7073%	73.0414%	71.5883%
$f = 0.40$	69.1223%	73.0528%	72.5419%

Table 1 displays the effects of nanoparticles of three types of noble metals NP's (Ag, Al, Au) showing that the highest absorption percentage occurs at $f = 0.40$ for Al metal and the lowest absorption occurs at $f = 0$ where NPs do not exist. We point out that different types of nanoparticles metals have distinct plasmonic resonance frequencies leading to different absorption spectra.

Comparing the numerical values given in Table 1 and Table 2 we see that higher absorption leads to lower reflection, thus when the absorption is increasing, the reflection is decreasing and *vice versa*.

Table 2

The reflection of metal nanoparticles (Ag, Al, Au) with different values of volume fraction (*f*)

Reflection %	Ag	Al	Au
$f = 0$	27.5109%	27.5109%	27.5109%
$f = 0.10$	24.778%	21.0626%	23.4594%
$f = 0.20$	21.3616%	18.1241%	20.2002%
$f = 0.30$	21.3967%	16.1739%	18.5469%
$f = 0.40$	21.2092%	15.7291%	17.7725%

Table 3 clearly shows the compression of the transmission due to different types of NPs in the front layer of the structure and that the Al is keeping the best value of transmission of all similar volume fractions of NPs.

Table 3

The transmission of metal nanoparticles (Ag, Al, Au) with different values of volume fraction (*f*)

Transmission %	Ag	Al	Au
$f = 0$	10.3036%	10.3036%	10.3036%
$f = 0.10$	10.0141%	10.4725%	10.0015%
$f = 0.20$	10.0716%	10.6248%	10.018%
$f = 0.30$	9.89605%	10.7847%	9.86478%
$f = 0.40$	9.66849%	11.2181%	9.68558%

Both reflection and transmission strongly depend on the nanoparticle volume fraction and the type of nanoparticles. The efficiency of solar cells can slightly be adjusted and tuned by varying either the volume fraction of the nanoparticles or the type of the metal in the front layer of the proposed cell structure.

4. CONCLUSION

In conclusion, this study proposes a new solar cell structure based on three types of nanoparticles. The absorption spectra have been investigated for Ag, Al, and Au, showing that the absorption spectra are increasing with the increasing of the volume fraction (*f*) of the nanoparticles. We have also noticed that the structure with aluminum metal (Al) has the best absorption enhancement. The obtained results show that the proposed solar cell structure could be considered as a promising design for the next-future generation of solar cells.

Acknowledgements. One of the authors (MMSh) acknowledges financial support from Alquds Academy for Scientific Research, Palestine, the financial support from DAAD, Germany, and the hospitability of Prof. Dr. Hartmut G. Roskos, Physikalisches Institut, Johann Wolfgang Goethe-Universität, Germany.

REFERENCES

1. J. Meier *et al*., *Efficiency enhancement of amorphous silicon p-i-n solar cells by LPCVD ZnO*, Conference Record of the Twenty-Eighth IEEE Photovoltaic Specialists Conference, 746–749 (2000).
2. B. L. Sopori and R. A. Pryor, Solar Cells **8**, 249 (1983).
3. M.A. Green, *Solar cells: Operating Principles, Technology, and System Applications*, Prentice-Hall series in solid state physical electronics (1982).
4. P. Würfel and U. Würfel, Physics of solar cells: from basic principles to advanced concepts, John Wiley & Sons (2009).
5. J. Nelson, The Physics of Solar Cells, vol. 57, Imperial College Press, U.K. (2003).
6. D. Redfield, Solar Cells **3**, 27 (1981).
7. M. M. Shabat, N. S. El-Samak, and D. M. Schaadt, Rom. Rep. Phys. **70**, 410 (2018).
8. M. M. Shabat, M. Ubeid, and M. A. Abu Rahma, Modern Phys. Lett. B **32** (15), 1850346 (2018).
9. H. Raether, Surface Plasmons, Springer, Germany (1988).
10. H. M. Mousa, M. M. Shabat, and A. K. Ouda, J. Science and Engineering B **7** (9–10), 229 (2017).
11. D. Qu, F. Liu, J. F. Yu, W. L. Xie, Q. Xu, X. D. Li, and Y. D. Huang, Appl. Phys. Lett. **98**, 113119 (2011).
12. M. F. Ubeid and M. M. Shabat, J. Modern Opt. **64** (4), 374 (2017).
13. H. M. Mousa, M. M. Shabat, and D. M. Schaadt, J. Electrical Engineering **5**, 288 (2017).
14. D. M. Schaadt, B. Feng, and E. T. Yu, App. Phys. Lett. **86**, 063106 (2005).
15. X. H. Li, P. C. Li, D. Z. Hu, D. M. Schaadt, and E. T. Yu, J. App. Phys. **115**, 044303 (2014).
16. H. J. El-Khozendar, R. J. El-Khozondar, M. M. Shabat, and D. M. Schaadt, Optik **166**, 127 (2018).
17. M. M. Shabat, D. M. El-Amassi, and D. M. Schaadt, Solar Energy Journal **137**, 409 (2016).
18. W. E. Sha, W. C. Choy, and W. C. Chew, Opt. Express **18** (6), 5993 (2010).
19. F. L. Pedrotti, L. S. Pedrotti, and L. M. Pedrotti, Introduction to Optics, 3rd ed. Upper Saddle River, NJ: Pearson Prentice Hall (2007).
20. H. Oraizi and M. Afsahi, Progress in Electromagnetics Research B **14**, 263 (2009).
21. H. Hamoucheand M. M. Shabat, App. Phys. A **122** (7), 1–7 (2016).
22. D. M. El-Amassi, H. J. El-Khozondar, and M. M. Shabat, Int. J. Nano Stud. Technol. **4**, 84–87 (2015).
23. D. M. Sullivan, *Electromagnetic simulation using the FDTD method*, John Wiley & Sons (2013).
24. A. Taflove, and S.C. Hagness, *Computational electrodynamics: the finite-difference time-domain method*. Norwood, 2nd Edition, MA: Artech House (l995).
25. K. H. Lee *et al.*, Progress In Electromagnetics Research **116**, 441 (2011).
26. G. Mur, IEEE Transactions on Electromagnetic Compatibility **4**, 377 (1981).
27. J.-P. Berenger, J. Computational Phys. **114** (2), 185 (1994).
28. F. Xu *et al*., IEEE Trans. on Microwave Theory and Techn. **51** (11), 2221 (2003).
29. E. D. Palik, *Handbook of Optical Constants of Solids*, Harcourt Brace Jovanovich, New York (1985).
30. A. D. Rakić, Appl. Opt. **34** (22), 4755–4767 (1995).
31. L. Genzel and T. P. Martin, Surf. Sci. **34**, 33 (1973).
32. P. B. Johnson and R. W. Christy, Phys. Rev. B **6** (12), 4370 (1972).
33. R. Ruppin, Opt. Commun. **182** (4–6), 273–279 (2000).
34. See, https://www.lumerical.com/tcad-products/fdtd/
35. H. Hamouche and M. M. Shabat, Appl. Phys. A **122**, 685 (2016).